Chemical Science

ROYAL SOCIETY OF CHEMISTRY

EDGE ARTICLE

View Article Online
View Journal | View Issue

Cite this: *Chem. Sci.*, 2025, **16**, 7411

All publication charges for this article have been paid for by the Royal Society of Chemistry

Received 25th November 2024
Accepted 17th March 2025

DOI: 10.1039/d4sc07959k

rsc.li/chemical-science

Reticular chemistry guided function customization: a case study of constructing low-polarity channels for efficient C_3H_6/C_2H_4 separation†

Jiantang Li, ‡[a] Zitong Song,‡[a] Xia Zhou,[a] Xue Wang,[a] Meng Feng,[a] Dongmei Wang*[a] and Banglin Chen *[ab]

Guided by the principles of reticular chemistry, we have successfully presented the "bending-bridge" strategy, achieving an extraordinary function-targeted assembly by ingeniously redirecting the coordination direction of traditional SBUs. This led to the synthesis of a novel metal–organic framework (MOF), {[CH_3NH_3][InTPCA]·$2H_2O$·NMF·DMF} (**ZJNU-401**). The smart design of bending branches within the ligand effectively transformed the tetrahedrally coordinated mononuclear In(III) into a square-planar configuration, thereby avoiding the introduction of open metal sites (OMSs) commonly associated with traditional ssb networks and creating a low-polarity pore surface environment. **ZJNU-401** exhibits an optimal pore system that enhances its efficacy for high uptake of C_3H_6 and C_2H_6 over C_2H_4. The remarkable selectivity ratio of C_3H_6 to C_2H_4 reaches up to 15.45, alongside efficient one-step purification of C_2H_4 (>99.95%) from the mixture of C_3H_6/C_2H_4. DFT calculations revealed that multiple O active sites within nonpolar pores provide stronger interactions with both C_3H_6 and C_2H_6 compared to those with C_2H_4.

Introduction

The methanol-to-olefin (MTO) process has become an important sustainable technology that allows non-petroleum resources to be converted into low-carbon olefins like ethylene (C_2H_4) and propylene (C_3H_6).[1–4] In the chemical industry, these olefins are essential raw materials, especially for the manufacture of polymers. The MTO method produces trace amounts of ethane (C_2H_6) impurities in addition to around 51 wt% C_2H_4 and 21 wt% C_3H_6.[5–7] The purification of MTO products is crucial for obtaining high-purity C_2H_4 and C_3H_6, which are necessary for the sustainability and effectiveness of the chemical manufacturing industry. The coexistence of these components in combination hampers downstream applications. However, it remains highly challenging to separate these gases due to their similar physical properties. Compared to traditional energy-intensive separation processes, physical adsorption technology based on porous materials offers a safer, more energy-efficient, and environmentally friendly alternative, presenting significant potential for sustainable molecular separations, particularly in the purification of MTO products.[8–10]

The rapid development of reticular chemistry has allowed the integration of various building blocks into extendable frameworks *via* strong bonds, leading to the emergence of novel porous materials such as metal–organic frameworks (MOFs).[11–17] Furthermore, reticular chemistry serves as a powerful strategy for tailoring specific pore environments and structures to achieve targeted separations. For instance, in the context of MTO product purification, the design of low-polarity pore surfaces enables weak interactions with certain molecules, facilitating effective kinetic separations. This approach has proven highly effective for distinguishing molecules with similar physical properties, such as olefins and alkanes.[18] Therefore, employing reticular chemistry to design MOFs with precisely tuned pore environments is not only necessary but also a promising pathway to optimize separation efficiency and address the challenges of sustainable chemical manufacturing.

Not all nets are ideal targets for reticular chemistry, which is an important consideration in MOF design. As is known to all, transitivity [pqrs] refers to a structure that has p types of vertexes, q types of edges, r types of faces, and s types of tiles. Edge-transitive nets, which have only one type of edge (q = 1), are quite important.[19,20] In 2021, Eddaoudi *et al.* identified 53 three-dimensional (3D) nets within this category that are particularly suitable for practical applications in reticular chemistry, being considered ideal candidates for the design and

[a]*Key Laboratory of the Ministry of Education for Advanced Catalysis Materials, College of Chemistry and Materials Sciences, Zhejiang Normal University, Jinhua 321004, P. R. China. E-mail: dmwang@zjnu.edu.cn*

[b]*Fujian Key Laboratory of Polymer Materials, College of Chemistry and Materials Sciences, Fujian Normal University, Fujian, 350007, P. R. China. E-mail: banglin.chen@fjnu.edu.cn*

† Electronic supplementary information (ESI) available. CCDC 2365428. For ESI and crystallographic data in CIF or other electronic format see DOI: https://doi.org/10.1039/d4sc07959k

‡ These authors contributed equally to this work.

construction of new structures.[15] One of the most important principles in constructing structures based on edge-transitive nets is building block selection, which includes the design of organic linkers as well as the selection of inorganic building units that are typically aligned with the desired functionality.[21–23] For example, the ssb net, which is a 4,4-c net formed by sql layers supported by pillars, has been realized using the Cu-paddlewheel and 4-c bulky organic linkers, as reported in NOTT-109 (ref. 24) and MMPF-1.[25] However, such designs pose challenges in creating low-polarity pore environments, as it is well known that Cu-paddlewheel SBUs provide abundant open metal sites (OMSs), which can be disadvantageous in certain separation applications, such as that of C_2H_6/C_2H_4.[26,27]

Developing an effective and controlled design strategy for assembling commonly used secondary building units (SBUs) that satisfies the functional needs while fulfilling the geometric requirements of specific topologies remains one of the most significant challenges in reticular chemistry.[28,29] Here, abandoning paddlewheel type SBUs, like Cu or Zn-paddlewheel, complicates the selection of alternative 4-c inorganic SBUs that can achieve square-planar connectivity. Other highly connected polynuclear metal SBUs, although possessing four connections, still do not meet functional requirements due to the presence of OMSs. A straightforward alternative is to use mononuclear metal SBUs based on single metal ions.[30,31] For achieving 4-c connectivity with carboxylate groups, In(III) stands out as an optimal choice, forming tetrahedral structures that are representative SBUs in ZMOFs.[32,33] These materials highlight the versatility of indium in creating robust frameworks without the complications associated with OMSs.

The next challenge is to transform these tetrahedral nodes into the square-planar 4-c nodes required by ssb nets. This is where the "bending-bridge" strategy in ligand design becomes essential. By introducing a well-planned bend at a specific point in the ligand, the directionality of coordination can be effectively altered. This enables the transformation of tetrahedral 4-c nodes into square-planar 4-c nodes, allowing them to conform to the structural requirements of the ssb network.[19,24] This approach offers a flexible and innovative pathway to achieve the desired geometry of the ssb net without compromising the integrity or functionality of the framework. Specifically, considering that the bending of the ligand results in a reduction of effective connection lengths, it is necessary to incorporate redundant space in the design of the bending bridges (Scheme 1). A symmetry-reduced ligand, H_4TPCA ([1,1′:3′,1″]terphenyl-3,4′,6′,3″-tetracarboxylic acid), has been employed in this system, taking into account two advantages: (1) the bending bridge can achieve large-angle rotations, thus adapting to the demands of the corresponding topology; and (2) the ligand integrates both the isophthalic acid part and the bending bridge part, allowing for a balance between rigidity and flexibility. Ultimately, as we anticipated, we truly succeeded in fabricating a low-polarity pore environmental compound (**ZJNU-401**) with the ssb network lacking OMSs. This facilitates the preferential selective adsorption of propylene and ethane (C_3H_6/C_2H_4: 15.45 and C_2H_6/C_2H_4: 1.75), thereby achieving efficient one-step separation and purification of ethylene (>99.95%) in the MTO process.

Results and discussion

Synthesis of ZJNU-401

$In(NO_3)_3 \cdot 4H_2O$ (8 mg, 0.021 mmol), H_4TPCA (3 mg, 0.074 mmol), *N*-methylformamide (NMF) (0.5 mL), *N*,*N*-dimethylformamide (DMF) (0.5 mL), deionized water (H_2O, 0.5 mL), and HNO_3 (500 μL, 2.2 mL of HNO_3 in 10 mL NMF) were mixed in a 20 mL vial and then placed in a precision oven for 12 h at 105 °C. After cooling to room temperature, colorless polyhedral crystals were collected and washed frequently with fresh NMF (yield 67.8%, based on H_4TPCA). Elemental analysis (%) Calcd for **ZJNU-401** {$[CH_3NH_3][InTPCA] \cdot 2H_2O \cdot NMF \cdot DMF$}: C, 46.86; H, 4.46; N, 5.86. Found: C, 47.01; H, 4.27; N, 5.80.

Crystal structure

Herein, the solvothermal reaction of a well-designed ligand, H_4TPCA, with $In(NO_3)_3 \cdot 4H_2O$, and HNO_3 in the DMF/NMF/H_2O system, enabled the construction of the targeted ssb net by employing the "bending-bridge" strategy. Single-crystal X-ray diffraction structural analysis reveals that **ZJNU-401** crystallizes in the rhombohedral crystal system with the *Fmm*2 space group where its asymmetric unit consists of eight In(III) ions, torsional deprotonated ligand $TPCA^{4-}$ and two $[CH_3NH_3]^+$ generated from the decomposition of NMF during solvothermal synthesis (Fig. S1†). As shown in Fig. 1a, the bending branch in the H_4TPCA ligand features a wider coordination angle compared to the H_4TPTA ligand, which can only rotate linearly. Additionally, the isophthalic acid part of the ligand coordinates with the metal In(III), occupying two of the four connectivities. The connections of the bending branches to the metal In(III), similar to a bending bridge, significantly alter the connection angle of the ligand, transforming the expected tetrahedrally coordinated mononuclear In(III) into a square-planar configuration. The asymmetric unit is illustrated by the crystal structure with a thermal ellipsoid diagram in Fig. S2.† This effective design strategy allows for the remarkable assembly of these two SBUs, which initially appear to be incompatible with the ssb topological node configuration, into the network. Moreover, in **ZJNU-401**, the introduction of open metal sites is effectively avoided, facilitating the formation of low-polarity pore surfaces. As shown in Fig. 1b and c, the bending branches of the ligand result in the straight channels being divided into a series of pockets, with a larger inner diameter of 11 Å and a smaller window size of 5 Å. Compared to the standard ssb network, **ZJNU-401** features a more diverse pore channel structure.

Thermal and chemical stability

The experimental PXRD results show good agreement with simulation data on crystallographic information (Fig. S3†), verifying phase purity and stability of the synthesized sample. The chemical resistance of **ZJNU-401** to water, HCl (aq, pH = 3) and NaOH (aq, pH = 11) was evaluated over a 12-hours period while maintaining an unchanged PXRD pattern. These tests

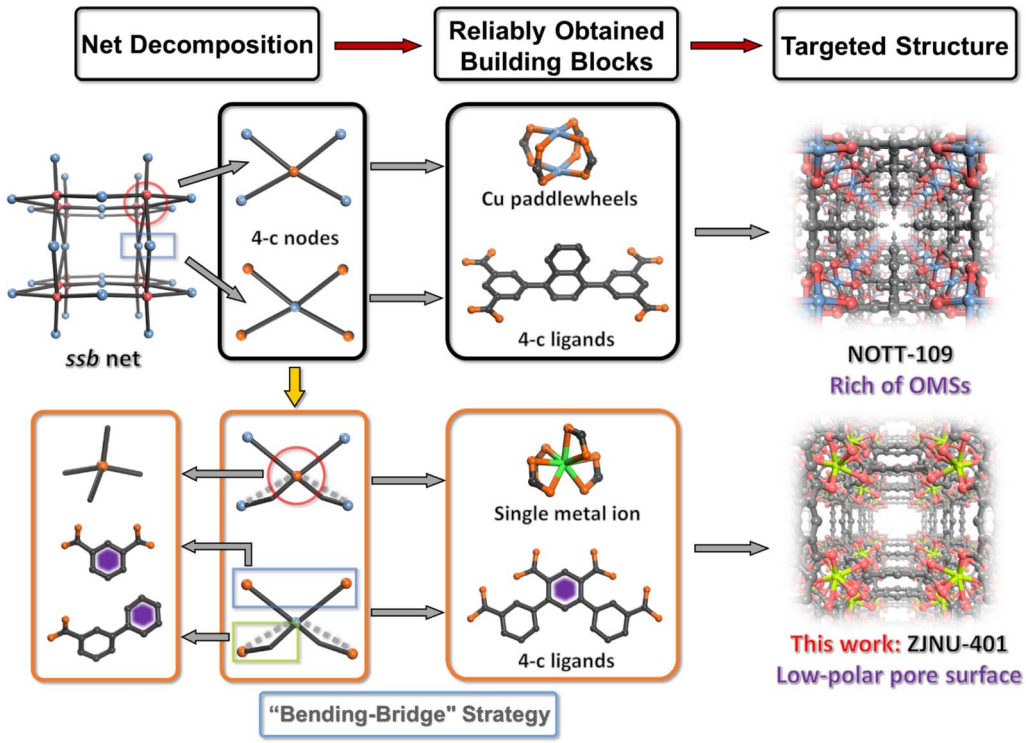

Scheme 1 Illustration of the "bending-bridge" strategy, which modifies the original design approach of the ssb net by utilizing mononuclear metals and the tetracarboxylic acid ligand to construct low-polarity pore surfaces.

demonstrate the robust chemical stability of the skeleton in both aqueous and harsh environments. Additionally, TGA analysis was conducted on **ZJNU-401** revealing an initial weight loss at 160 °C attributed to the removal of solvent molecules. Thermal decomposition commences when the temperature exceeds 300 °C resulting in the formation of corresponding oxides (Fig. S4†). These findings confirm the excellent chemical stability of **ZJNU-401**.

Gas adsorption of ZJNU-401

The permanent porosity of **ZJNU-401** was investigated through nitrogen adsorption at 77 K, which exhibited a reversible type-I adsorption isotherm with a maximum saturated uptake capacity and Brunauer–Emmett–Teller (BET) values of 280 cm^3 g^{-1} and 1224 m^2 g^{-1}, respectively. Pore size distribution was determined using the density functional theory (DFT) method (Fig. S5†). Notably, JLU-MOF121 with twofold interpenetrated

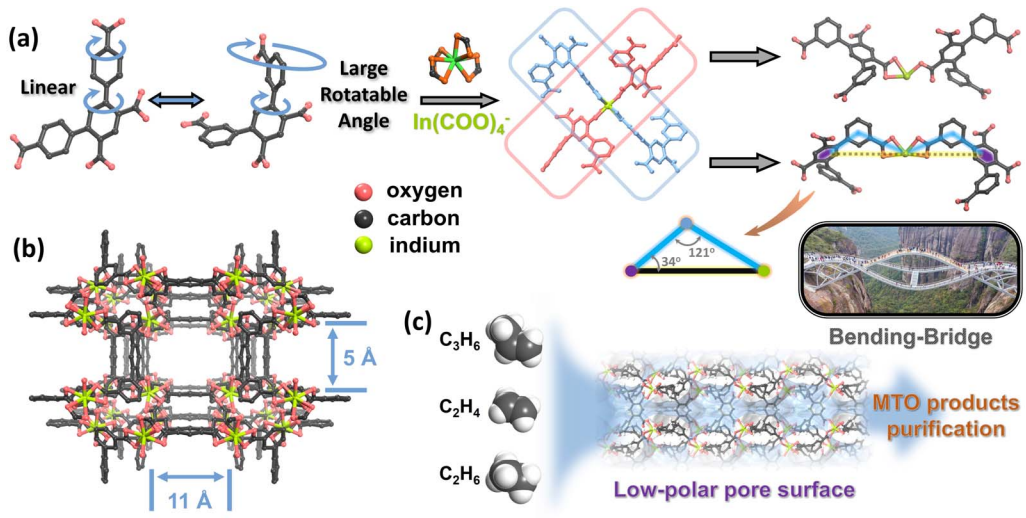

Fig. 1 Structural description of **ZJNU-401**: (a) from the "bending-bridge" design of the ligand to the assembly with mononuclear In^{3+} to form the 4-c node; (b) 1D pore channel of **ZJNU-401**; (c) low-polarity pore surface for effective MTO product purification.

and In-TPTAB with oversized pores did not exhibit any N_2 adsorption behavior.[34,35] The unique pore environment characteristics of **ZJNU-401**, including uncoordinated O atoms, a saturated metal coordination mode, and an appropriate pore size, render it a promising candidate for investigating gas adsorption and separation properties.[36,37] Consequently, one-component adsorption isotherms for C_3H_6, C_2H_4 and C_2H_6 were evaluated at 273/298/308 K under 1 bar. As illustrated in Fig. 2a–c and S6,† **ZJNU-401** demonstrates exceptional adsorption capacities of 5.38/4.53/4.28 mmol g^{-1} for C_3H_6 and 4.74/3.43/3.05 mmol g^{-1} for C_2H_6, both significantly higher than that of 4.51/2.94/2.57 mmol g^{-1} for C_2H_4. These results can be attributed to the smaller molecular size and fewer hydrogen atoms present in C_2H_4, leading to weaker host–guest interactions compared to the other gases studied.[38–40] In Fig. S5,† especially in the low-pressure region, the affinity of **ZJNU-401** for C_3H_6, C_2H_6 and C_2H_4 shows a decreasing trend. This is consistent with the results of their respective adsorption enthalpies Q_{st} (C_3H_6) = 32 kJ mol^{-1}, Q_{st} (C_2H_6) = 29 kJ mol^{-1}, Q_{st} (C_2H_4) = 19 kJ mol^{-1} as depicted in Fig. S7.†

IAST selectivity and breakthrough testing of ZJNU-401

Remarkably, the adsorption capacity of **ZJNU-401** for C_3H_6 and C_2H_6 is significantly higher than that for C_2H_4, underscoring its suitability as an effective adsorbent material for the purification of C_2H_4, particularly in MTO processes. Consequently, we employed ideal adsorption solution theory (IAST) to calculate the separation of equimolar two-component gas mixtures at temperatures of 273/298/308 K under 100 kPa. As illustrated in Fig. 2d and S8, S9,† **ZJNU-401** exhibited favourable selectivity values of 1.69/1.75/1.56 for C_2H_6/C_2H_4. This enhanced selectivity can be attributed to the slightly higher polarizability of C_2H_6 (44.7×10^{25} cm^3) and more hydrogen atoms compared to that of C_2H_4 (42.52×10^{25} cm^3). Furthermore, exceptional selectivity values of 11.81/15.45/13.96 were achieved for C_3H_6/C_2H_4, surpassing those reported for many well-known compounds in this field. Moreover, our calculations indicate that **ZJNU-401** holds significant promise for efficiently purifying C_2H_4 from gas mixtures to yield polymer-grade olefin products. A comparison of **ZJNU-401**'s separation results at three different temperatures reveals that 298 K provides optimal purification conditions. Thus, a dynamic breakthrough experiment was conducted at this temperature and pressure using activated **ZJNU-401** to separate mixtures of $C_3H_6/C_2H_6/C_2H_4$ (v/v/v, 1/1/1) and C_3H_6/C_2H_4 (v/v, 1/1) (Fig. 2e and f). The carrier gas used was Ar with a total flow rate of 2 mL min^{-1}. Initially, C_2H_4 elutes from the packed column at around 28 min while no detection of C_3H_6 occurs until approximately 87 min. As a result, high-purity C_2H_4 (>99.95%) can be continuously obtained over an extended duration lasting up to 59 min. Furthermore, while good adsorption is desirable, good repeatability is essential for the practical application of porous adsorbents. We performed multiple cycles of adsorption using C_2H_4 gas and the breakthrough experiment after exposed to air for two months, and performed adsorption tests after six hours of immersion in different acid–base solutions (Fig. S10–S12†). The results indicate that **ZJNU-401** remains virtually unchanged, thereby confirming its excellent reproducibility. These findings underscore the

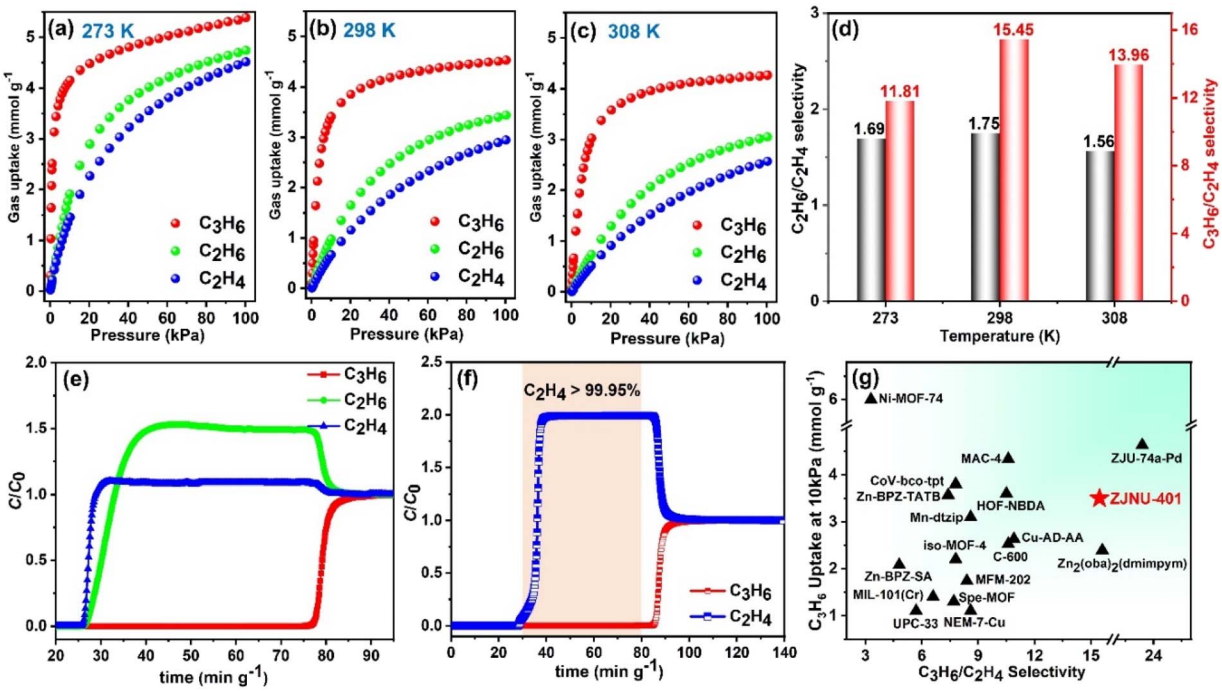

Fig. 2 (a–c) The adsorption isotherms of C_3H_6, C_2H_4 and C_2H_6 at 273/298/308 K under 1 bar; (d) the selectivity of equimolar mixtures of C_2H_6/C_2H_4 and C_3H_6/C_2H_4 at 273/298/308 K; (e and f) the breakthrough curves of $C_3H_6/C_2H_6/C_2H_4$ (v/v/v, 1/1/1) and C_3H_6/C_2H_4 (v/v, 1/1) mixtures in an adsorber bed packed with activated **ZJNU-401** at 298 K and 1 bar; (g) comparison of selectivity for C_3H_6/C_2H_4 and C_3H_6 adsorption capacity at 10 kPa with other reported MOFs at 298 K.

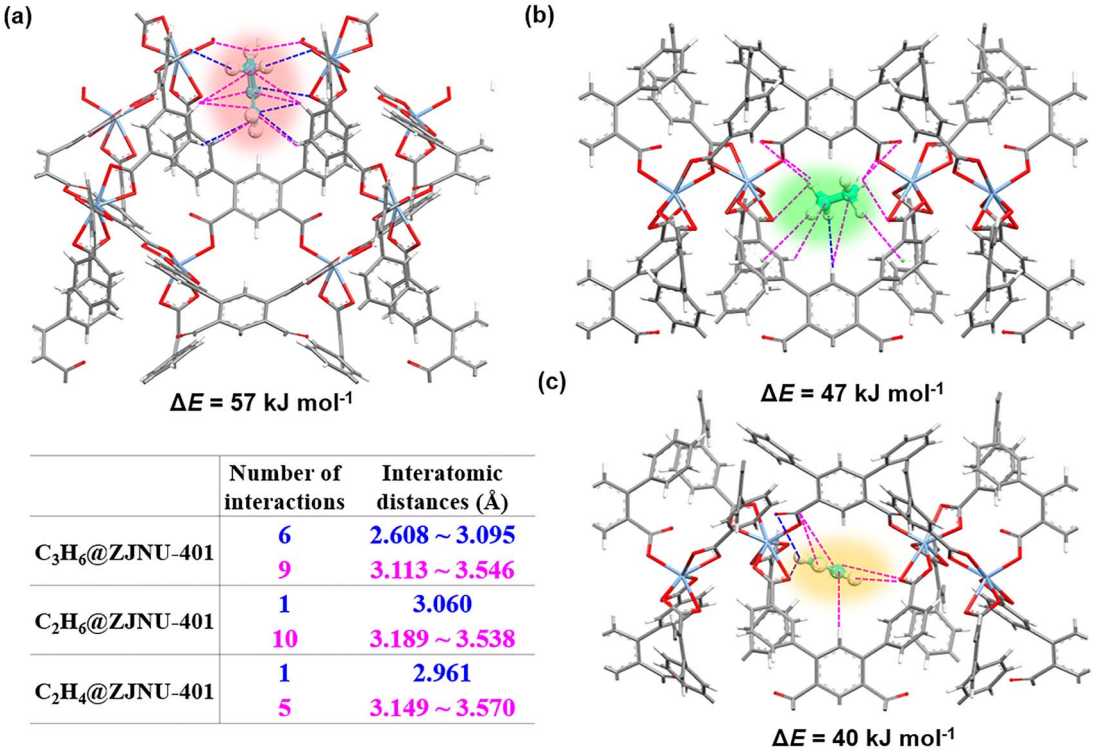

	Number of interactions	Interatomic distances (Å)
C_3H_6@ZJNU-401	6	2.608 ~ 3.095
	9	3.113 ~ 3.546
C_2H_6@ZJNU-401	1	3.060
	10	3.189 ~ 3.538
C_2H_4@ZJNU-401	1	2.961
	5	3.149 ~ 3.570

Fig. 3 Calculation of the optimized adsorption sites for (a) C_3H_6 and (b) C_2H_6 and (c) C_2H_4 within **ZJNU-401**, and comparison of the host–guest interactions among them.

potential applicability of **ZJNU-401** as an excellent material for industrial MTO product separation. In Fig. 2g, we compare selectivity for both C_3H_6/C_2H_4 and C_3H_6 adsorption capacity at a pressure level of 10 kPa against other reported MOFs at 298 K.[41–55] Notably, **ZJNU-401** demonstrates considerable advantages in addressing the recognized "trade-off" dilemma.

Theoretical simulation

To gain further insights into the host–guest interactions between the framework and the adsorbate, the fixed loading task in the Sorption module based on the metropolis Monte Carlo method in MS 2020 was employed to determine the adsorption sites of acetylene, ethane and ethylene molecules at the MOF of **ZJNU-401**. Subsequently, binding energy between the adsorbates and framework was calculated for the low energy structure obtained from adsorption site calculation. As illustrated in Fig. 3 and S13,† the optimal adsorption sites for olefins are located near the $[In(COO)_4]^-$ cluster within the channel, while alkanes tend to be surrounded by nonpolar aromatic rings. In **ZJNU-401**, we observed that all three gases interact with aromatic carboxylic acid backbones through multiple C–H···O/C hydrogen bonds and C–H···π interactions. For C_3H_6, there are six short H···C/O distances ranging from 2.608 to 3.095 Å, which is significantly greater than those of C_2H_6 and C_2H_4, resulting in a stronger binding affinity. This enhanced interaction can be attributed to the larger polarizability and size of the propylene molecule, which facilitates more extensive interactions with the framework (Fig. S14†). In contrast to C_2H_4, the saturated hydrocarbon C_2H_6 has a higher number of hydrogen atoms. Thus, it is more likely to be trapped by low-polarity benzene rings, forming approximately twice as many interactions at distances from 3.189 to 3.538 Å. Moreover, the host–guest binding energies are calculated as ΔE (C_3H_6) = 57 kJ mol^{-1}, ΔE (C_2H_6) = 47 kJ mol^{-1}, and ΔE (C_2H_4) = 40 kJ mol^{-1}, respectively. These results indicate that both the low-polarity pore surface of **ZJNU-401** and the intrinsic properties of the gases are conducive to the selective capture of C_2H_4 from mixtures containing C_3H_6/C_2H_4 and C_2H_6/C_2H_4. Finally, a comparison of the bond lengths of corresponding parts in the calculated structure and the host-crystal structure of **ZJNU-401** was carried out. Since **ZJNU-401** is a rigid framework, gas adsorption has a negligible influence on the host-crystal structures, resulting in insignificant bond-length changes (Fig. S15†).

Conclusions

In summary, the introduction of a strategically designed bending angle at a specific point in the ligand facilitates the formation of square-planar 4-c nodes, providing a flexible and innovative pathway to achieve the desired geometry of the ssb net. The low polarity pore surfaces with accessible O active sites endow **ZJNU-401** with preferential adsorption for C_3H_6 and C_2H_6 over C_2H_4, resulting in significant selectivity of C_3H_6/C_2H_4 (15.45) and C_2H_6/C_2H_4 (1.75). High-purity C_2H_4 (>99.95% pure) was produced from C_3H_6/C_2H_4 mixtures with a low-energy footprint. Multiple cycle experiments confirm its excellent reproducibility. DFT calculation results show that both the quantity and strength of host–guest interactions synergistically enhance the affinity of **ZJNU-401** for C_3H_6 and C_2H_6 over C_2H_4.

This work establishes **ZJNU-401** as a benchmark MOF for challenging binary separations involving C_2H_6/C_2H_4 and C_3H_6/C_2H_4, while also providing valuable insights to facilitate the design of ideal target nets based on advanced reticular chemistry for application in C_2H_4 purification.

Data availability

The authors confirm that the data supporting the findings of this study are available within the article [and/or its ESI†].

Author contributions

Jiantang Li: writing – original draft, supervision; Zitong Song: preparation and synthesis of materials; Xia Zhou: experimental data analysis; Xue Wang: validation, visualization; Meng Feng: resources, software; Dongmei Wang: writing – review & editing, supervision, data curation; Banglin Chen: writing – review & editing, supervision.

Conflicts of interest

There are no conflicts to declare.

Acknowledgements

This work was supported by the National Natural Science Foundation of China (52102189, 22301154 and W2431013) and the Jinhua City Project (2023-4-019).

Notes and references

1 L. Hengbo, Z. Yunzhe, C. Cheng, L. Yashuang, L. Zheng, W. Mingyan and H. Maochun, *Inorg. Chem.*, 2024, **63**, 21548–21554.
2 P. Tian, Y. Wei, M. Ye and Z. Liu, *ACS Catal.*, 2015, **5**, 1922–1938.
3 M. Yang, D. Fan, Y. Wei, P. Tian and Z. Liu, *Adv. Mater.*, 2019, **31**, 1902181.
4 G.-D. Wang, Y.-Z. Li, W.-J. Shi, L. Hou, Y.-Y. Wang and Z. Zhu, *Angew. Chem., Int. Ed.*, 2022, **61**, e202205427.
5 C. Wang, L. Yang, M. Gao, X. Shao, W. Dai, G. Wu, N. Guan, Z. Xu, M. Ye and L. Li, *J. Am. Chem. Soc.*, 2022, **144**, 21408–21416.
6 A. Cesarini, S. Mitchell, G. Zichittella, M. Agrachev, S. P. Schmid, G. Jeschke, Z. Pan, A. Bodi, P. Hemberger and J. Pérez-Ramírez, *Nat. Catal.*, 2022, **5**, 605–614.
7 Z. Belohlav, P. Zamostny and T. Herink, *Chem. Eng. Process.*, 2003, **42**, 461–473.
8 G. Zhen, Y. Liu, Y. Zhou, Z. Ji, H. Li, S. Zou, W. Zhang, Y. Li, Y. Liu, C. Chen and M. Wu, *ACS Appl. Mater. Interfaces*, 2024, **16**, 1179–1186.
9 R. Qin, Z. Zhao, N. Shi, G. Chen, M. Yang, Q. Ren, H. Ji and K. Chai, *Microporous Mesoporous Mater.*, 2024, **373**, 113134.
10 Z. Di, Z. Ji, C. Chen, R. Krishna, D. Yuan, M. Hong and M. Wu, *Chem. Eng. J.*, 2024, **493**, 152442.
11 O. M. Yaghi, M. O'Keeffe, N. W. Ockwig, H. K. Chae, M. Eddaoudi and J. Kim, *Nature*, 2003, **423**, 705–714.
12 R. Freund, S. Canossa, S. M. Cohen, W. Yan, H. Deng, V. Guillerm, M. Eddaoudi, D. G. Madden, D. Fairen-Jimenez, H. Lyu, L. K. Macreadie, Z. Ji, Y. Zhang, B. Wang, F. Haase, C. Wöll, O. Zaremba, J. Andreo, S. Wuttke and C. S. Diercks, *Angew. Chem., Int. Ed.*, 2021, **60**, 23946–23974.
13 W. Xu, B. Tu, Q. Liu, Y. Shu, C.-C. Liang, C. S. Diercks, O. M. Yaghi, Y.-B. Zhang, H. Deng and Q. Li, *Nat. Rev. Mater.*, 2020, **5**, 764–779.
14 Z. Chen, K. O. Kirlikovali, P. Li and O. K. Farha, *Acc. Chem. Res.*, 2022, **55**, 579–591.
15 V. Guillerm and M. Eddaoudi, *Acc. Chem. Res.*, 2021, **54**, 3298–3312.
16 H. Jiang, D. Alezi and M. Eddaoudi, *Nat. Rev. Mater.*, 2021, **6**, 466–487.
17 O. M. Yaghi, *Nano Lett.*, 2020, **20**, 8432–8434.
18 R.-B. Lin, H. Wu, L. Li, X.-L. Tang, Z. Li, J. Gao, H. Cui, W. Zhou and B. Chen, *J. Am. Chem. Soc.*, 2018, **140**, 12940–12946.
19 M. Li, D. Li, M. O'Keeffe and O. M. Yaghi, *Chem. Rev.*, 2014, **114**, 1343–1370.
20 Z. Chen, H. Jiang, M. O'Keeffe and M. Eddaoudi, *Faraday Discuss.*, 2017, **201**, 127–143.
21 L. Liu and S. G. Telfer, *J. Am. Chem. Soc.*, 2015, **137**, 3901–3909.
22 B. Zheng, J. Bai, J. Duan, L. Wojtas and M. J. Zaworotko, *J. Am. Chem. Soc.*, 2011, **133**, 748–751.
23 J. Li, P. M. Bhatt, J. Li, M. Eddaoudi and Y. Liu, *Adv. Mater.*, 2020, **32**, 2002563.
24 X. Lin, I. Telepeni, A. J. Blake, A. Dailly, C. M. Brown, J. M. Simmons, M. Zoppi, G. S. Walker, K. M. Thomas, T. J. Mays, P. Hubberstey, N. R. Champness and M. Schröder, *J. Am. Chem. Soc.*, 2009, **131**, 2159–2171.
25 X.-S. Wang, L. Meng, Q. Cheng, C. Kim, L. Wojtas, M. Chrzanowski, Y.-S. Chen, X. P. Zhang and S. Ma, *J. Am. Chem. Soc.*, 2011, **133**, 16322–16325.
26 B. Li, Y. Zhang, R. Krishna, K. Yao, Y. Han, Z. Wu, D. Ma, Z. Shi, T. Pham, B. Space, J. Liu, P. K. Thallapally, J. Liu, M. Chrzanowski and S. Ma, *J. Am. Chem. Soc.*, 2014, **136**, 8654–8660.
27 L. Zhang, L. Li, E. Hu, L. Yang, K. Shao, L. Yao, K. Jiang, Y. Cui, Y. Yang, B. Li, B. Chen and G. Qian, *Adv. Sci.*, 2020, **7**, 1901918.
28 M. O'Keeffe and O. M. Yaghi, *Chem. Rev.*, 2012, **112**, 675–702.
29 M. J. Kalmutzki, N. Hanikel and O. M. Yaghi, *Sci. Adv.*, 2018, **4**, 9180.
30 V. Kumar Maka, P. Tamuly, S. Jindal and J. Narasimha Moorthy, *Appl. Mater. Today*, 2020, **19**, 100613.
31 Y.-Q. Zhang, L. Liu, W.-Z. Li, B.-H. Wu, C.-N. Li, J.-Q. Chu and Z.-B. Han, *Inorg. Chem.*, 2024, **63**, 7705–7713.
32 M. Eddaoudi, D. F. Sava, J. F. Eubank, K. Adil and V. Guillerm, *Chem. Soc. Rev.*, 2015, **44**, 228–249.
33 M. H. Alkordi, J. A. Brant, L. Wojtas, V. C. Kravtsov, A. J. Cairns and M. Eddaoudi, *J. Am. Chem. Soc.*, 2009, **131**, 17753–17755.

34 Y. Zhu, J. Cai, L. Xu, G. Li and Y. Liu, *Inorg. Chem.*, 2022, **61**, 10957–10964.
35 M. Feng, L. Wu, X. Wang, J. Wang, D. Wang and C. Li, *Appl. Organomet. Chem.*, 2022, **36**, e6546.
36 F. Meng, L. Jiantang, W. Xirong, W. Jingyu, W. Dongmei and C. Banglin, *Inorg. Chem. Front.*, 2024, **11**, 7947–7954.
37 Q. Ding, Z. Zhang, Y. Liu, K. Chai, R. Krishna and S. Zhang, *Angew. Chem., Int. Ed.*, 2022, **61**, e202208134.
38 W. Gang-Ding, C. Jing, L. Yong-Zhi, H. Lei, W. Yao-Yu and Z. Zhonghua, *Chem. Eng. J.*, 2021, **433**, 133786.
39 Y. Ye, Y. Xie, Y. Shi, L. Gong, J. Phipps, A. M. Al-Enizi, A. Nafady, B. Chen and S. Ma, *Angew. Chem., Int. Ed.*, 2023, **62**, e202302564.
40 Z. Wang, Y. Zhang, E. Lin, S. Geng, M. Wang, J. Liu, Y. Chen, P. Cheng and Z. Zhang, *J. Am. Chem. Soc.*, 2023, **145**, 21483–21490.
41 W. Jia-Xin, Z. Teng-Fei, P. Jiyan, L. Di, W. Yu-Bo, G. Xiao-Wen, Q. Guodong and L. Bin, *Chem Bio Eng.*, 2024, **1**, 952–959.
42 Y.-Z. Li, G.-D. Wang, R. Krishna, Q. Yin, D. Zhao, J. Qi, Y. Sui and L. Hou, *Chem. Eng. J.*, 2023, **466**, 143056.
43 Y. Zhou, C. Chen, Z. Ji, R. Krishna, Z. Di, D. Yuan and M. Wu, *ACS Mater. Lett.*, 2024, **6**, 1388–1395.
44 H. Lyu, J. Zhu, B. Zhou, H. Cao, J. Duan, L. Chen, W. Jin and Q. Xu, *Carbon*, 2018, **139**, 740–749.
45 G.-D. Wang, Y.-Z. Li, R. Krishna, W.-Y. Zhang, L. Hou, Y.-Y. Wang and Z. Zhu, *Angew. Chem., Int. Ed.*, 2024, **63**, e202319978.
46 L. Zhang, L.-N. Ma, G.-D. Wang, L. Hou, Z. Zhu and Y.-Y. Wang, *J. Mater. Chem. A*, 2023, **11**, 2343–2348.
47 S. Gao, C. G. Morris, Z. Lu, Y. Yan, H. G. W. Godfrey, C. Murray, C. C. Tang, K. M. Thomas, S. Yang and M. Schröder, *Chem. Mater.*, 2016, **28**, 2331–2340.
48 X. Liu, C. Hao, J. Li, Y. Wang, Y. Hou, X. Li, L. Zhao, H. Zhu and W. Guo, *Inorg. Chem. Front.*, 2018, **5**, 2898–2905.
49 Y. Xiao, A. N. Hong, Y. Chen, H. Yang, Y. Wang, X. Bu and P. Feng, *Small*, 2023, **19**, 2205119.
50 G.-D. Wang, Y.-Z. Li, W.-J. Shi, L. Hou, Y.-Y. Wang and Z. Zhu, *Angew. Chem., Int. Ed.*, 2023, **62**, e202311654.
51 W. Fan, X. Wang, X. Zhang, X. Liu, Y. Wang, Z. Kang, F. Dai, B. Xu, R. Wang and D. Sun, *ACS Cent. Sci.*, 2019, **5**, 1261–1268.
52 H. Fang, B. Zheng, Z.-H. Zhang, H.-X. Li, D.-X. Xue and J. Bai, *Angew. Chem., Int. Ed.*, 2021, **60**, 16521–16528.
53 G. Chang, M. Huang, Y. Su, H. Xing, B. Su, Z. Zhang, Q. Yang, Y. Yang, Q. Ren, Z. Bao and B. Chen, *Chem. Commun.*, 2015, **51**, 2859–2862.
54 W. Fan, Y. Wang, Q. Zhang, A. Kirchon, Z. Xiao, L. Zhang, F. Dai, R. Wang and D. Sun, *Chem. –Eur. J.*, 2018, **24**, 2137–2143.
55 G.-D. Wang, R. Krishna, Y.-Z. Li, Y.-Y. Ma, L. Hou, Y.-Y. Wang and Z. Zhu, *ACS Mater. Lett.*, 2023, **5**, 1091–1099.